Mon. Not. R. Astron. Soc. **000**, 000–000 (0000) Printed 11 November 2014 (MN LATEX style file v2.2)

GRAVIMAGE II: Non-parametric modelling of dwarf spheroidals

P. Steger[1⋆], J. I. Read[2]
[1] *Institute for Astronomy, Department of Physics, ETH Zürich, Wolfgang-Pauli-Strasse 27, CH-8093 Zürich, Switzerland*
[2] *Department of Physics, University of Surrey, Guildford, GU2 7XH, UK*

11 November 2014

ABSTRACT
We show applications of the new mass modelling tool GRAVIMAGE to observed dwarf galaxies, Fornax, Sculptor, Sextans, Carina, and Draco.

Key words: galaxies: dwarf – galaxies: fundamental parameters – galaxies: kinematics and dynamics – cosmology: dark matter

1 INTRODUCTION

2 METHOD

We employ the non-parametric mass modelling described in (**?**):

The total mass density is given in bins by setting the density slope

$$n(r_j) = -\mathrm{d}\ln\rho(r)/\mathrm{d}\ln r|_{r=r_j} \quad (1)$$

for $j...N_{\rm bin}$ radial bins: $1 \leqslant j \leqslant N_{\rm bin}$, and interpolated linearly in between bin radii $r_{{\rm min},j} < r < r_{{\rm max},j}$.

The density then is given by

$$\rho(r) = \rho_{1/2} \cdot \exp\left[-\int_{\ln r_{1/2}}^{\ln r} n(s)\mathrm{d}s\right],$$

with the density at half-light radius $\rho(r_{1/2}) = \rho_{1/2}$, We prescribe three buffer bins $n(r_j)$ for $j \in \{N_{\rm bin}+1, N_{\rm bin}+2, N_{\rm bin}+3\}$ outside of the range where data is given to enable sensible extrapolations towards high radii, and two additional slopes $n_0 < 3, n_\infty > 3$ for the asymptotic density slopes towards $r = 0$ and $r = \infty$, which are reached at half the smallest radius and $r_\infty = 10 r_{\rm max}$.

2.1 Splitting Populations

Observations of the abundances of metals and chemical species in the stellar atmospheres show that the ensemble of stars in a dwarf galaxy or globular cluster can be split into populations.

An approach by Walker & Peñarrubia (2011) showed that if the population of e.g. Fornax is split into two populations, and each of their half-light radius and mass are determined, restrictions on the overall potential can be drawn. Using this approach, they prefer a cored DM profile for Fornax.

For real data, we will use a splitting based on metallicity. This is achieved by using a separate Markov Chain Monte Carlo method. The overall metallicity distribution is represented by a sum of two Gaussians with means $\mu_{1,2}$ and widths $\sigma_{1,2}$, and each stellar tracer with metallicity M is assigned a population based on the likelihood of its metallicity belonging to said population. The process is repeated to marginalize over the means and widths of the metallicity distributions. A sample splitting result is shown in fig. 1.

We restrict the method to Mg indices only, as the iron measurements in Walker & Peñarrubia (2011) are not reliable enough, and a sizeable fraction has no metallicity measurements.

Walker & Peñarrubia (2011) assume a Plummer-like profile for both populations, which must be dropped in our non-parametric profile. We additionally let drop the velocity information, and concentrate on non-kinematic properties of the stars only. Foreground stars are accounted for by weighting the probabilities of membership in each population with the overall dSph probability of membership.

We first assume two populations, and from the pdf of the Mg indices, we calculate the tracer density profiles for both populations. Each star contributes to both populations, with a fraction given by its probability of belonging to the chemical population i.

If we then see no significant difference between the half-light radii distribution of all models with two populations, we conclude that population splitting for that particular galaxy will not give us a significant information gain in GRAVIMAGE .

If we on the other hand get a distinct peak in the pdf of the half-light radii we know that there are two – or possibly more – distinct populations we can use for further analysis.

Optimally, we assign each star randomly in proportion

⋆ E-mail: psteger@phys.ethz.ch

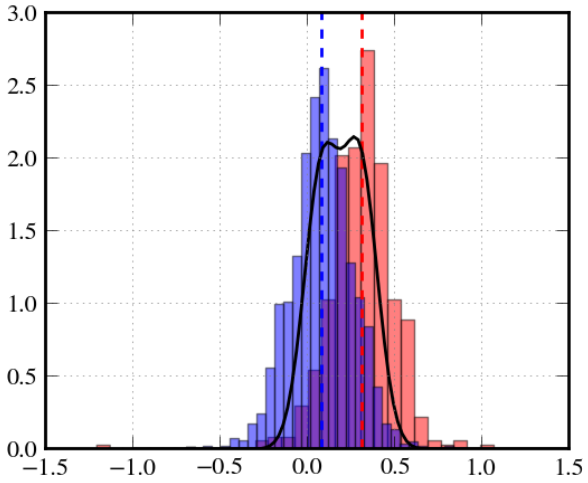

Figure 1. Reconstruction of two populations from mock data. The underlying metallicity distributions are shown as red and blue histograms. The retrieved centers of the Gaussians are shown as vertical lines, and the reconstructed metallicity distribution is depicted as black line.

to f_i to population i for each step in the MultiNest procedure.

2.2 Detailed Explanation

In our test suite there are dwarf galaxies with different scale radii and small differences in the mean of the metallicity for the two populations of stars. In order to reproduce the underlying populations we use an inset MCMC with assumptions that

(i) Foreground stars are younger than most of the dSph member stars. Therefore, they show a high metallicity and can be removed from the dataset with a single cut in metallicity;
(ii) the remaining stellar components are divided into two populations;
(iii) the fraction of stars in population 1 is sampled in a uniform way in the range $[0, 1]$;
(iv) both populations show a normal distribution in metallicity with an individual width;

To test whether the assignment into populations is a valid one, we want to check whether the population is in equilibrium with the overall potential.

The routine then assigns each particle to one of the two populations, based on its Mg metallicity. $75 \pm 4\%$ of all stars are assigned to the correct underlying distribution on a mock dataset from the Gaia challenge. This in turn changes the half-light radius by 110pc and -62pc for initial 390 pc, 730 pc half light radii. These changes are rather high, but the two populations still show distinct half-light radii.

We explicitly assume two populations of stellar tracers in dwarf galaxies, each with Gaussian distributions in metallicity with means μ_1, μ_2. Without requiring a minimum distance $\delta\mu = \mu_2 - \mu_1$ between them, a representation with $\mu_1 \approx \mu_2$ can be found. This model shows a higher χ^2 than other models and is thus disfavoured, but cannot be rejected from a Kolmogorov-Smirnov test on a $p < 0.05$ basis.

Here we show the influence of setting a prior minimal $\delta\mu_{\rm min}$ on the goodness of fit, and the allowed range of $\delta\mu$. We work on the metallicity distribution of one of the mock dwarfs with cusped density profiles described earlier on, setting

$$\mu_1 \in [-1.0, 2.0]; \quad \delta\mu \in [\delta\mu_{\rm min}, 5.0]; \tag{2}$$

with $\delta\mu_{\rm min}$ varying from 0.0 to 0.4. We let the MCMC run for a) 10k iterations with 8k burn-in/discarded models; b) 50k iterations with 40k burn-in. From the accepted models, we compute the mean Gaussian distributions and compare the corresponding overall bimodal distribution to the actual metallicity distribution from the data with a 2 component Kolmogorov-Smirnov test, and take the two-tailed statistics p_{KS} from 30 drawings. If $p_{KS} > 0.05$, then we cannot reject the hypothesis that the distributions of the two samples are the same.

Results for varying the minimal distance between the two Gaussians between 0.0 and 0.4 are shown in fig 2.

All models with $p > 0.05$ give a reasonable fit, with a maximum for 10k iterations at around $\delta\mu = 0.1$. Models with $\delta\mu > 0.2$ give no good fit anymore after 10k iterations.

The goodness of fit is enhanced if we take more iterations, so in the plot for 50k iterations, there is a maximum $p = 0.79$ compared to $p = 0.4$ from 10k iterations only. The whole curve is shifted to higher $\delta\mu$ values. The models with $\delta\mu > 0.3$ are rejected. The restriction of $\delta\mu > 0.4$ (last point to the right) is well-fitting again, but this is due to the fact that the fraction of particles for population 2 was found to be smaller than 10 percent, thus mainly fitting the metallicity distribution with one Gaussian only, plus some skewing from an almost negligible stellar component. Although this model cannot be rejected, it lies above the rejected models at $\delta\mu_{\rm min} = 0.4$. Furthermore, it does not yield a second component with a scale length distinctly different from the main component, rendering the additional gain from two components obsolete. Thus, we will restrict the MCMC search of the population fraction to the range $f \in [0.3, 0.7]$.

2.3 Baryonic Density Profiles

Our Jeans-based method finds constraints on the overall mass density profile

$$\rho_{\rm tot} = \rho_{\rm DM} + \rho_{\rm bary} \tag{3}$$

where $\rho_{\rm DM}$ is the dark matter density profile, and $\rho_{\rm bary}$ is the baryonic density profile. As we are mostly interested in the dark matter, we need to subtract the baryonic contribution.

As the kinematic data we have is rather sparse – not each star in the dSph has its LOS velocity measured – and misses other contributions like gas, we subtract a photometrically defined baryonic density.

The errors on this density are rather small, thus we only use the deprojected 3D photometric density profile for the subtraction, without sampling over its errors, as is done for the kinematic tracer population profiles.

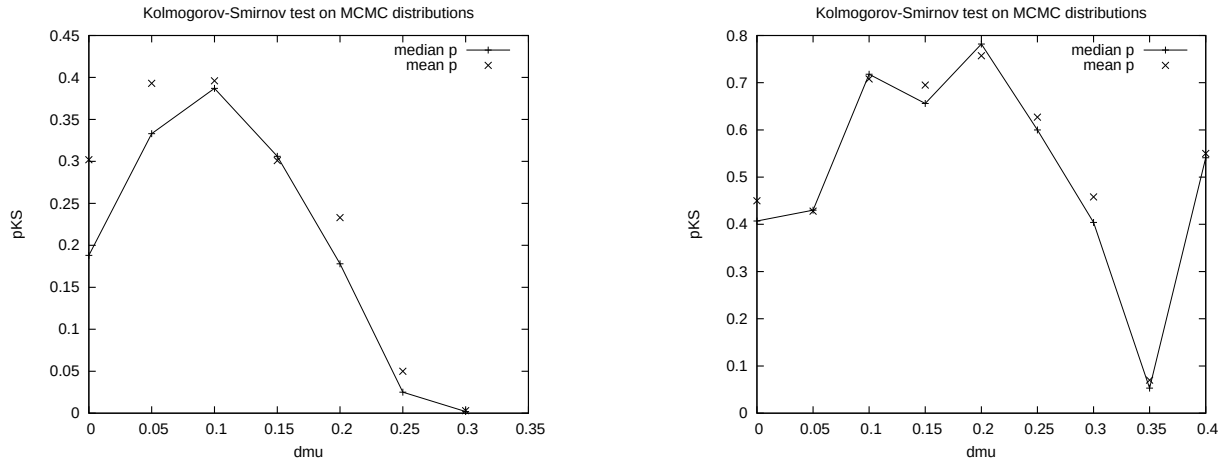

Figure 2. Kolmogorov-Smirnov test statistic p_{KS} for correspondance between models with $\delta\mu > \delta\mu_{\rm min}$ as described in the text.

3 DATA

3.1 Fornax

(TODO: ref) find evidence for three populations.

We use the photometric data for the overall baryonic profile from **?**.

3.2 Sculptor

3.3 Carina

3.4 Sextans

3.5 Draco

4 RESULTS

TODO: chi^2 distribution, Sigma, sigma

TODO: Sextans

5 CONCLUSIONS

The new non-parametric method samples the profiles of the overall density bin-wise, and was shown to reconstruct the density of diverse mock data.

6 ACKNOWLEDGEMENTS

JIR would like to acknowledge support from SNF grant PP00P2_128540/1.

REFERENCES

Walker M. G., Peñarrubia J., 2011, ApJ, 742, 20

7 APPENDIX

7.1 Effect of Wrong Assignment of Populations

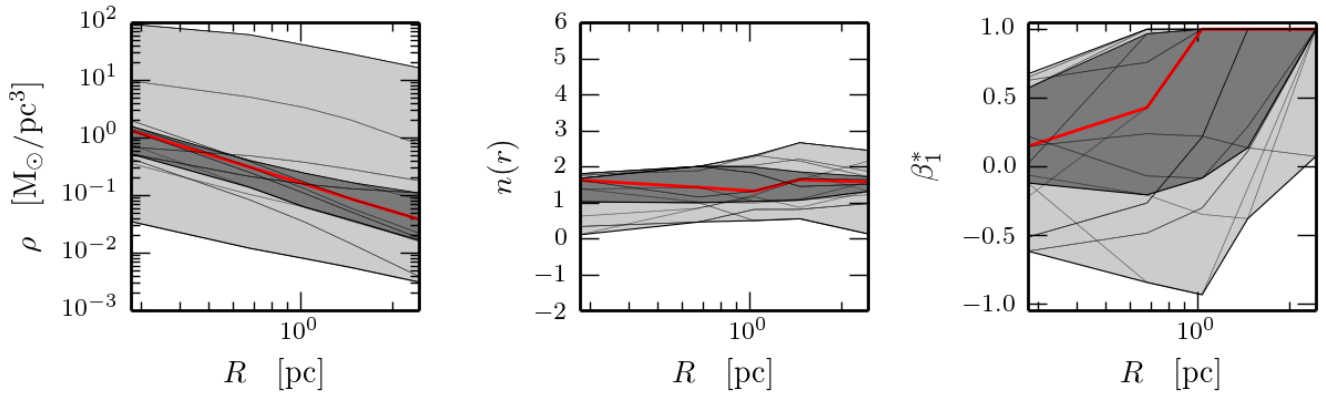

Figure 3. Reconstructed density, density slope, and velocity anisotropy of Fornax (red shows median, shaded areas show the 68 and 95 percentiles) for TODO tracer particles, after TODO iterations. The vertical lines give the projected half-light radius (for 2D quantities), and the half-light radius for the median model for 3D quantities.

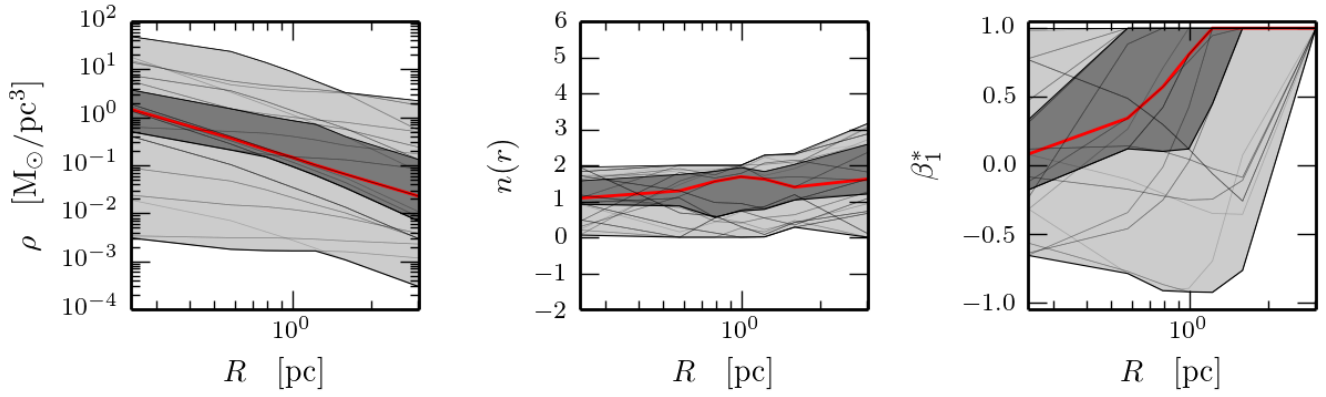

Figure 4. Reconstructed density, density slope, and velocity anisotropy of Carina (red shows median, shaded areas show the 68 and 95 percentiles) for TODO tracer particles, after TODO iterations. The vertical lines give the projected half-light radius (for 2D quantities), and the half-light radius for the median model for 3D quantities.

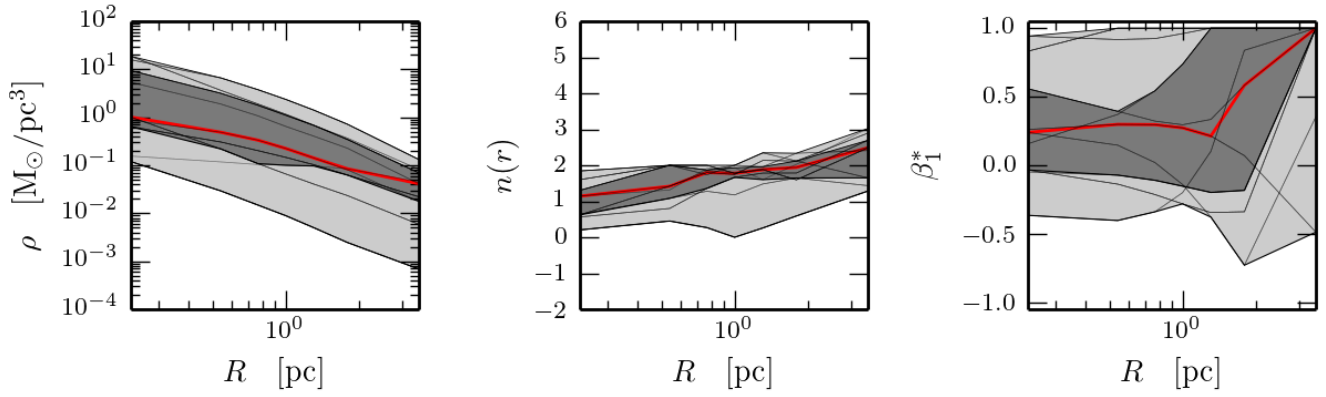

Figure 5. Reconstructed density, density slope, and velocity anisotropy of Sculptor (red shows median, shaded areas show the 68 and 95 percentiles) for TODO tracer particles, after TODO iterations. The vertical lines give the projected half-light radius (for 2D quantities), and the half-light radius for the median model for 3D quantities.